Simulation of radiation damage in silicon sensors

Summer Student 2013

Anna Tampellini

Abstract

The aim of this report is to explain the reasons for studying silicon sensors, to shortly describe how a simulation works and finally to summarize the results concerning simulations of silicon sensors affected by radiation damage. In my study I've used 2D simulations with the purpose of analyzing how sensors parameters, like leakage current, electric field and inner capacitances, may be changed by x ray and hard particles radiations.

Contents

1 Introduction

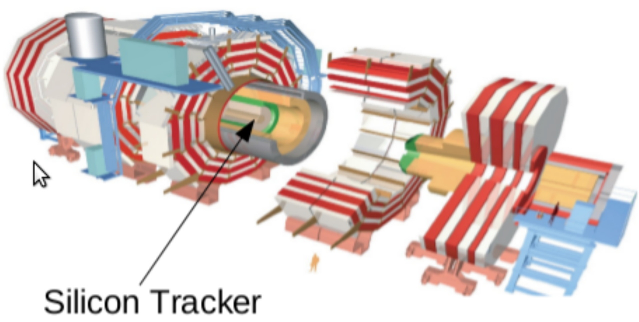

Figure 1: CMS tracker

The current CMS tracker was built for 10 years run time (500 fb^{-1}) and for peaks of instantaneous luminosity of 1034 cm^{-1} s^{-1}. With the next LHC upgrade instantaneous luminosity will increase by a factor of five and a harsher radiation environment will be created. Therefore new radiation harder sensors are needed for the CMS tracker. In order to study radiation effects on silicon sensors, a powerful tool is simulation. It allows to study the inner work of a sensor and to analyze how its physical properties are changed by radiation damage.

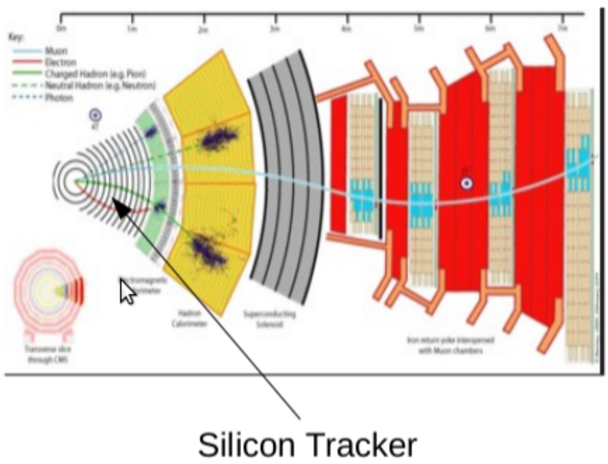

Figure 2: structure CMS tracker

As shown in the folowing diagram (Figure.3) particles fluence is expected to depend on the tracker radius. Since the silicon tracker with strip sensors is located in the inner part of the tracker (Figure.2) the expected radiation is up to a fluence of 1e16 $/cm^2$. Nevertheless a first analysis will concern fluence values between $1e^{14}$ and $1e^{15}/cm^2$.

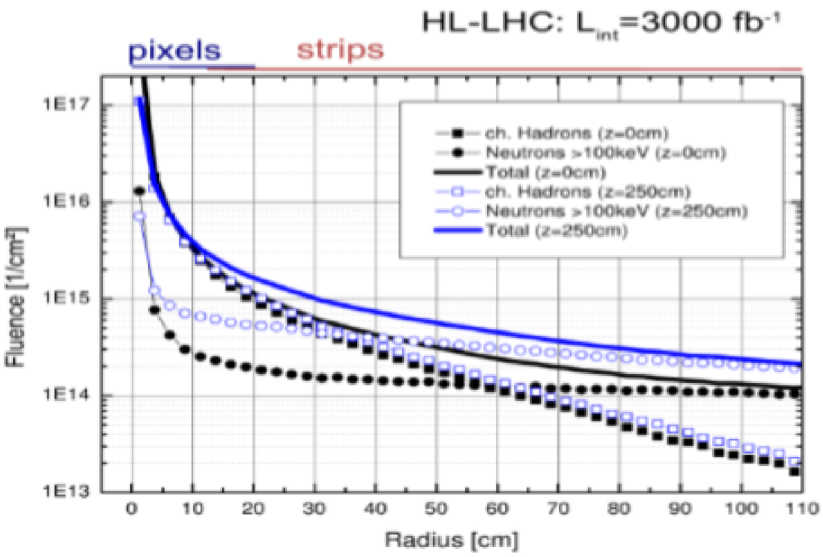

Figure 3: expected radiation

2 TCAD simulations

The software used for sensor simulations is Synopsys Sentaurus TCAD.

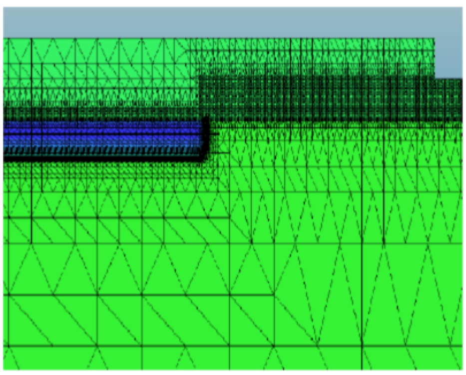

Figure 4: simulation of a strip corner

The simulation procedure consists of different steps:

1. The sensor structure is generated by defining geometry, used materials and their properties such as doping concentration for silicon;
2. Additional physical properties are given to the sensor (temperature, charge carriers mobility, trapping...);
3. To run the simulation a grid is built on the defined sensor (Figure.4), the mesh might have different sizes depending on the region of the sensor: interfaces or sections with non constant doping profile need smaller mesh to be analyzed;
4. Different kind of simulations are available; in order to analyze currents or electric fields a simple I-V simulation in DC can be used, to study capacitances an AC simulation is needed;
5. At each previously generated mesh point of the grid Poisson's

   $$\frac{d^2V(x)}{dx^2} = -\frac{\rho(x)}{\epsilon_r \epsilon_0}$$

   equation and carrier continuity equation

   $$\vec{\nabla} J_n = q\left(R_{eff} + \frac{\partial n}{\partial t}\right)$$

   $$-\vec{\nabla} J_p = q\left(R_{eff} + \frac{\partial p}{\partial t}\right)$$

   are solved;
6. Simulation data about physical properties (like charge distribution, electric field...) are extracted from the solution of the two equations;

3 Silicon sensors

3.1 n type sensors

3.1.1 Structure

The structure of the sensor used in simulations is the following (Figure.5, Figure.6):

layers	thickness	width	doping concentration
Aluminum	1µm -1.32µm	28µm	-
SiO_2	1 µm	240 µm	-
P strip	1.5 µm	20µm	5e18/cm2
Silicon bulk	320 µm	240 µm	-
Active region (in silicon bulk)	120 µm/ 320 µm	240 µm	3.5 e12 /cm2
backplane	5 µm	240 µm	5e18 /cm2

Figure 5: simulation parameter

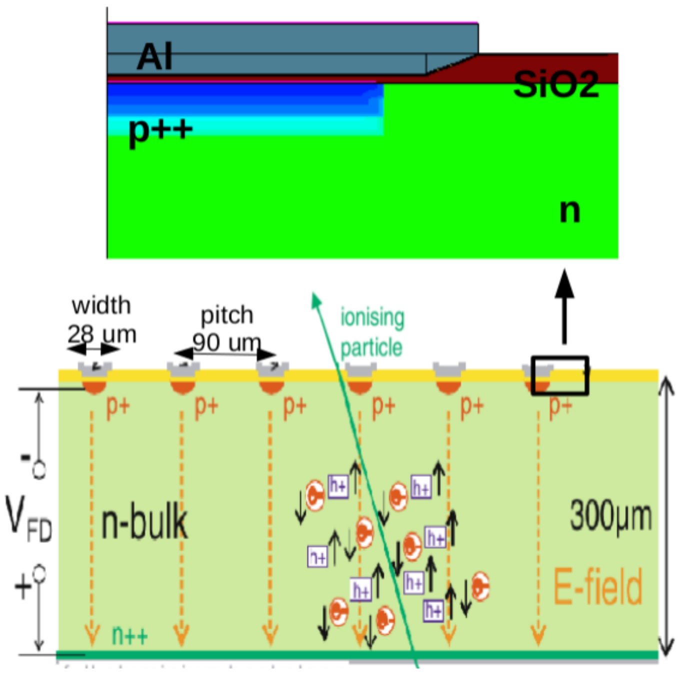

Figure 6: n type sensor structure

simulations will be done with sensors with both 120 μm and 320 μm active region in order to compare sensors with different thickness.

3.1.2 Working principles

Through the addition of electrodes both on the top and on the bottom of the sensor a bias voltage can be applied. The sensor works in reverse bias condition so that the bulk can be fully depleted by free charge carriers. When a ionizing particle crosses the sensor, electron-hole pairs are generated. Electrons drift along the electric field toward the n backplane while holes are collected on the doped p strips. This positive charges are then induced by the capacitive coupling of the oxide layer to the aluminum readout strips generating the signal.

3.2 p type sensors

In order to study and compare different kind of sensors, p type sensors have been used as well. The structure and the working principles are the same as n type. Only doping type in bulk and implantations are exchanged and the bias voltage polarization is inverted in order to deplete the p bulk. Furthermore two p implantations are introduced between strips, in order to avoid cross talk, since electrons are now attracted by possible positive charge in the oxide interface.

4 Radiation damage

The sensor now has to be implemented with a model reproducing radiation damage in order to study radiation effects on the sensor working.

Radiation damage has to be distinguished into two different effects. The first, concerning the oxide layer is due to x-rays, the second one, concerning the silicon bulk, depends on hard radiation fluence.

4.1 Surface damage

The creation of electron/hole pairs by x-rays traversing the oxide layers is not fully reversible since SiO_2 is an insulator. Especially when a voltage is applied, holes drift to the $Si - SiO_2$ interface, generating a permanent concentration of positive charges. Some of them can be captured by existing defects in the oxide. This originates a positive charge distribution in the whole layer.

In order to simulate this effect, fixed charges will be added both to the oxide layer and, more specifically, to the silicon-oxide interface. Simulation will be run for different charge concentrations in a range between 0 and 3e12/cm2.

4.1.1 SiO_2 chrages and $SiO_2 - Si$ interface charges

First simulations concern a constant charge concentration in the interface ($1e^{12}/cm^2$) and different charge values in the oxide, in order to test the effect of trapped charges. While comparing simulations of the sensor behavior implemented with a charge concentration between $1e^{12}/cm^2$ and $3e^{12}/cm^2$, no differences have been seen nor in current neither in electric field profile. This means that this kind of trapping effect doesn't damage significantly the work of the sensor. For further simulations the charge concentration in oxide will be kept at a value of $1e^{12}/cm^2$.

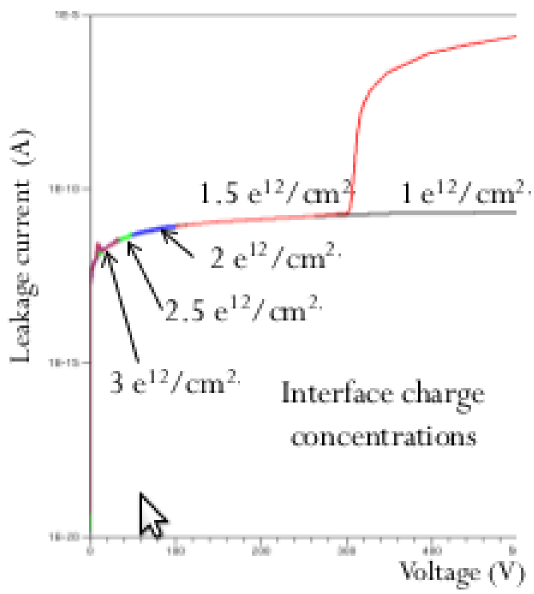

Figure 7: Leakage current vs voltage with Sentaurus Inspect

On the contrary, increasing the interface charge concentration, simulations give quite different results. As we can see in the previous diagrams (Figure.7), the I-V profile remains the same, but simulations break at low voltage for high charge concentration.

Since simulations break for high charge concentration, in order to study the sensor with bias voltage in a useful range, at least 0-300V, the following simulations will concern only charge values from 0 to $1.5e^{12}/cm^2$.

The physical properties which we are interested to analyze are leakage current, electric field and capacitances, since their alteration is the largest source of noise or failure of the signal.

4.1.2 Leakage current

The first physical property we need to check is the dark current, in order to test if the increasing amount of charges in the interfaces leads to a increasing noise in the outgoing signal.

In the following graph (Figur.8)the current intensity is plotted at 250V:

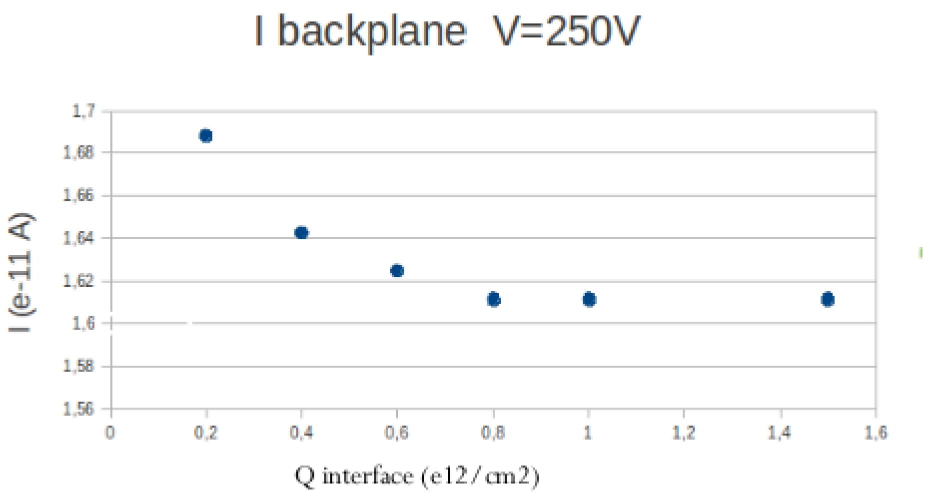

Figure 8: Leakage current at V=250V

Considering that the current intensity is in the order of magnitude of e^{-11}A, the decrease shown on the diagram can be ignored and the leakage current, as expected, can be considered independent from radiation effects in the oxide.

4.1.3 Electric field

As far as the electric field is concerned, in the following pictures (Figure.9) the electric field distribution in the sensor is represented for different interface charges.

In particular, the pictures show the region of the sensor between two strips. Since the strip-by-strip insulation is completely defined by the electric field distribution, we are deeply interested in studying it in this section of the sensor.

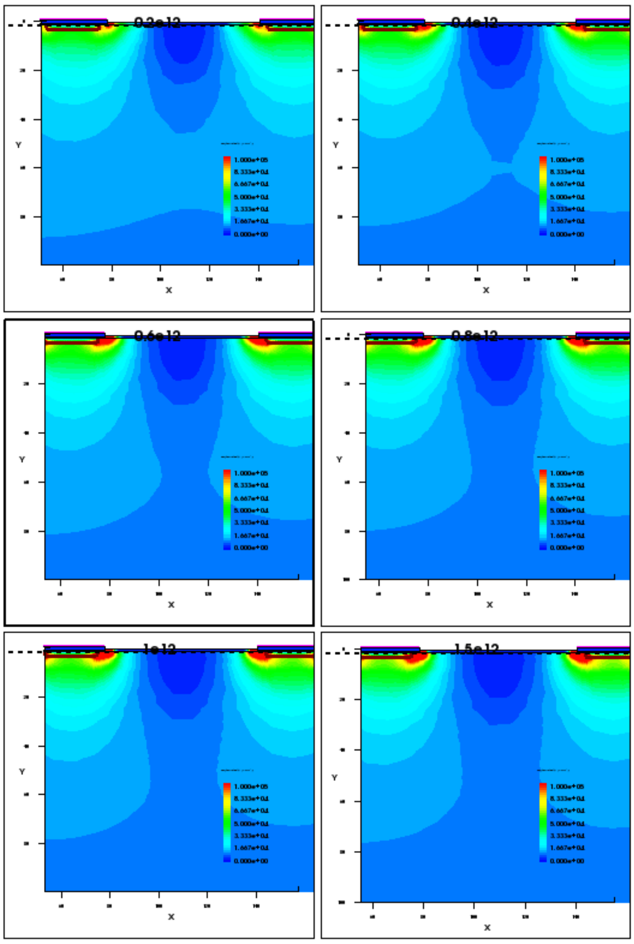

Figure 9: Electric field with Sentaurus Visual

From these histograms we can deduce an increase of the electric field in the strip corner and a decrease in the middle between the two strips. In order to analyze more precisely this behaviour, electric field vs charge concentration are plotted in the following diagrams. Electric field data are taken at a voltage of 250V, the highest possible before the 1.5e12/cm2 simulation break, at (78,4) for the maximum value of the strip corner (Figure.10) and at position (109,4) for the minimum value in the middle of the strips (Figure.11).

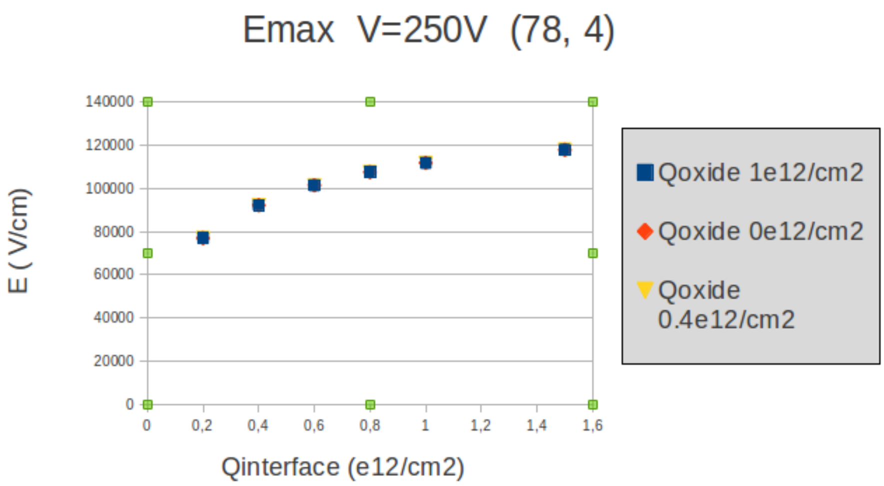

Figure 10: Electric field in (78,4)

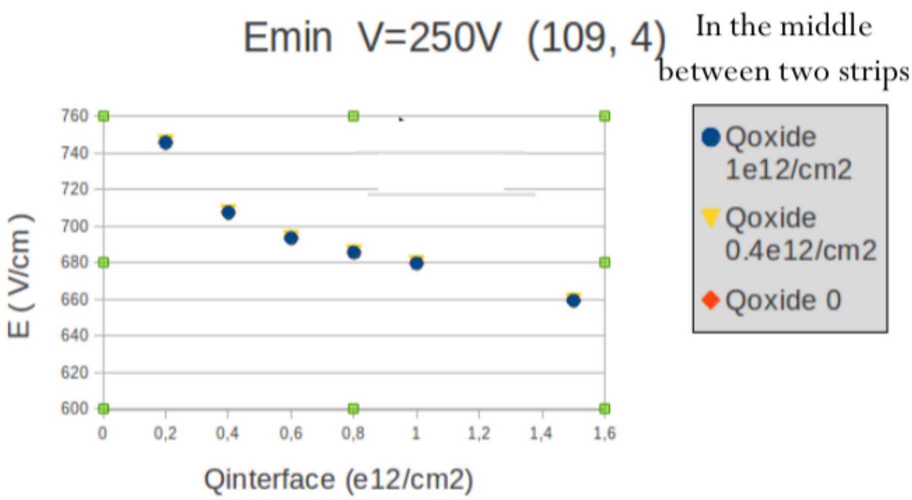

Figure 11: Electric field in (109,4)

4.1.4 Capacitances

Furthermore inner capacitances of the sensor are responsible of the failure of the sensor itself:

1. Backplane capacitance: between the bottom and the top of the silicon bulk. It's not expected to change very much with oxide damage since bulk properties are not changed. Checking the capacitance vs voltage profile is the quickest way to study the full depletion voltage of the sensor.

2. Coupling capacitance: between the implant and the aluminum readout strip. It should be large, being directly proportional to the signal. A large capacitance means a thin isolation layer which is sometimes difficult to achieve.

3. Interstrip capacitance: it's supposed to be smaller than the coupling capacitance to get most of the signal into the preamplifier. On the other hand, it shouldn't be too small, in order to increase spatial resolution by distributing signal to direct neighbours strips. For this reason the expected value should be 1 pF/cm. This value is expected to increase, producing additional noise, according to the formula: $C = \epsilon_0 \epsilon_r \frac{A}{d}$ since with the charge increase the depletion region between strips decreases.

In the following diagrams are reported capacitances vs charge concentration(Figure.12, Figur.13, Figure.13). The capacitance values are taken as usual at a voltage of 250V. On the same diagram capacitance of p-type and n-type sensor are compared. Furthermore for both coupling and backplane capacitance there are two data series, taken for capacitances concerning the first (lateral) and the second (central) strip, in order to test possible side effects.

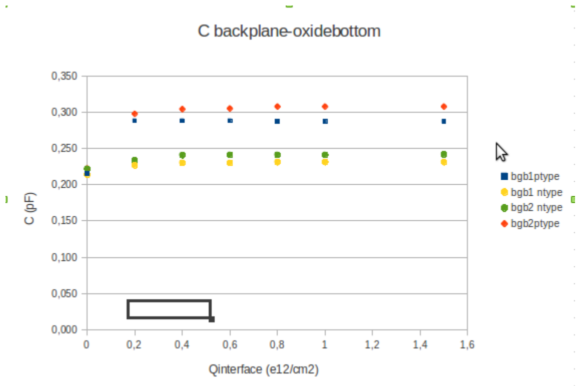

Figure 12: Backplane capacitance

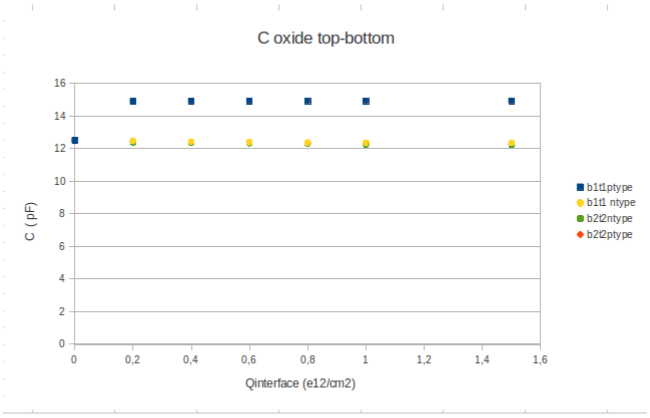

Figure 13: Coupling capacitance

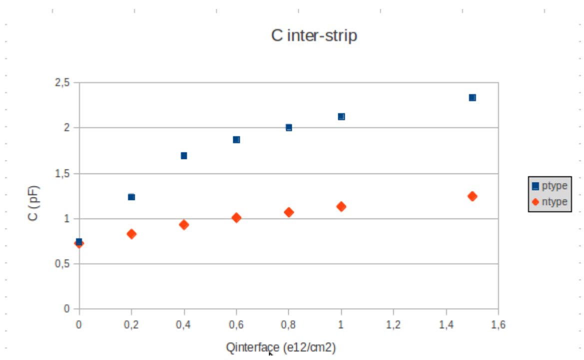

Figure 14: interstrip capacitance

analyzing the plots we can conclude:

1. Capacitance in p-type sensors are always higher than in n-type.
2. As expected the backplane and the coupling capacitances don't increase with interface charges, since they are not affected by increasing the amount of positive charges. Nevertheless we can assert that they are in the expected order of magnitude.
3. Concerning the interstrip capacitance, it increases as expected, but again around the predicted value.

As a consequence of this first analysis, a charge concentration of $1.5e^{12}/cm^2$ will be added to the silicon-oxide interface, while simulating radiation damage in the silicon bulk.

4.2 Bulk damage

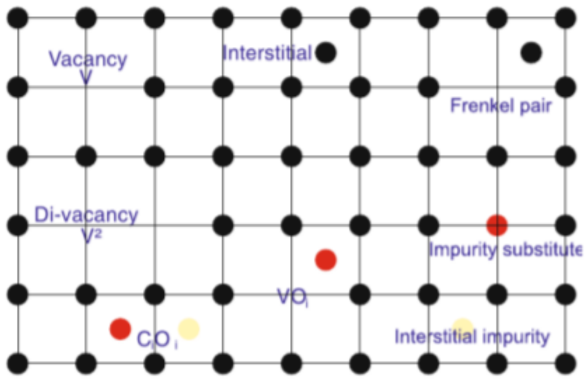

Figure 15: creation of lattice defects

Traversing particles deform the lattice by creating interstitials and vacancies (Figure.15). All these defects populate new level (Figure.16) in the energy gap that act as traps for drifting electrons and holes. A trap model has been developed in order to implement this effects on simulations. Since this model is meant to be a first approximation of the damage effects it consists in the addition of only two kind of traps. The parameters defining the traps are in the table below.

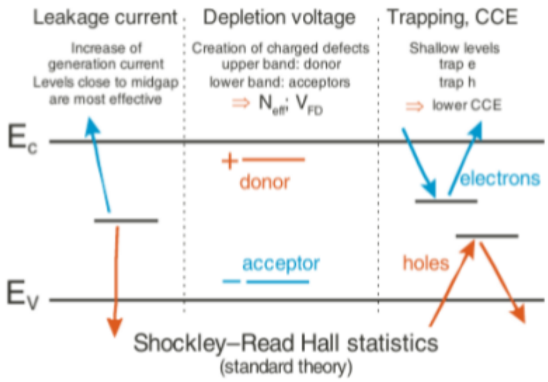

Figure 16: creation of new enery levels

Radiation type	Defect	Energy [eV]	σ[cm^{-2}]	g [cm]
proton	Acceptor	$E_c - 0.525$	e-14	1.189
	Donor	$E_V + 0.48$	e-14	5.598
neutron	Acceptor	$E_c - 0.525$	1.2e-14	1.55
	Donor	$E_V + 0.48$	1.2e-14	1.395

Figure 17: trap model parameters

The aim of this model is also to reproduce the electric field's double peak observed in irradiated sensors.

A brief explanation of the effect is the following:

Although the density of current j, crossing the sensor, is constant (Figure.18, a), their electron and hole components j_n and j_p are linearly distributed in the bulk (b) . Consequently, the concentrations of free carriers, which are proportional to the current components are linearly distributed in the detector(c). This non-uniform free carrier distribution, in detector with high concentration of traps, leads to a evenly non-uniform distribution of traps. Assuming concentration of trapped carriers to be proportional to the concentration of free carriers, it becomes clear that charge concentration will follow the profile of picture (d). Finally, as it follows from the Poisson equation

$$\frac{d^2V(x)}{dx^2} = -\frac{\rho(x)}{\epsilon_r \epsilon_0}$$

two peaks in E(x) appear next to the contacts (e).

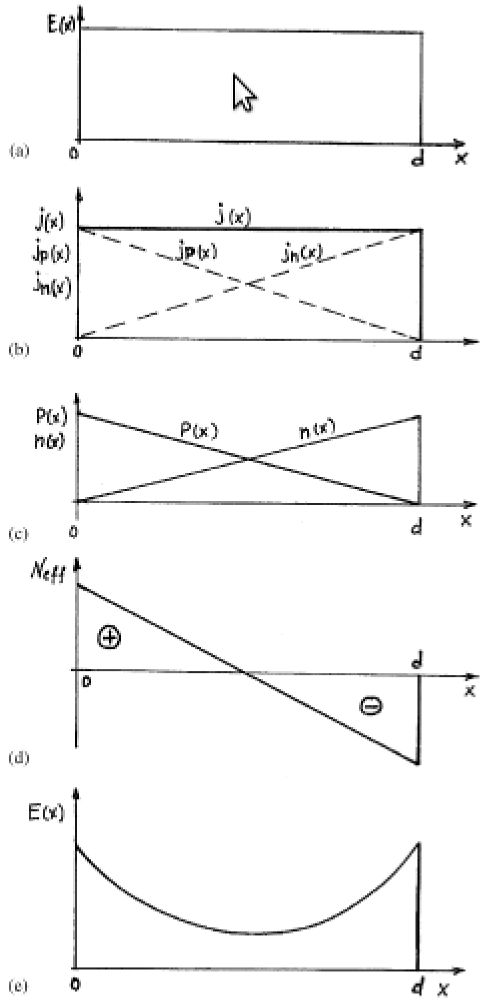

Figure 18:

In order to compare different kind of sensors and radiations, the model has been implemented both in n-type and p-type sensors irradiated by charged hadrons (protons) or neutrons.

4.2.1 Leakage current

The first Physical property to be analyzed is again leakage current. In the following diagram (Figure.19)the current profile is shown for increasing voltage at different fluence levels. Current intensity increases with fluence, keeping the same profile as dark current for fluence level of 0 and e^{12}/cm^2 (expected not to damage)

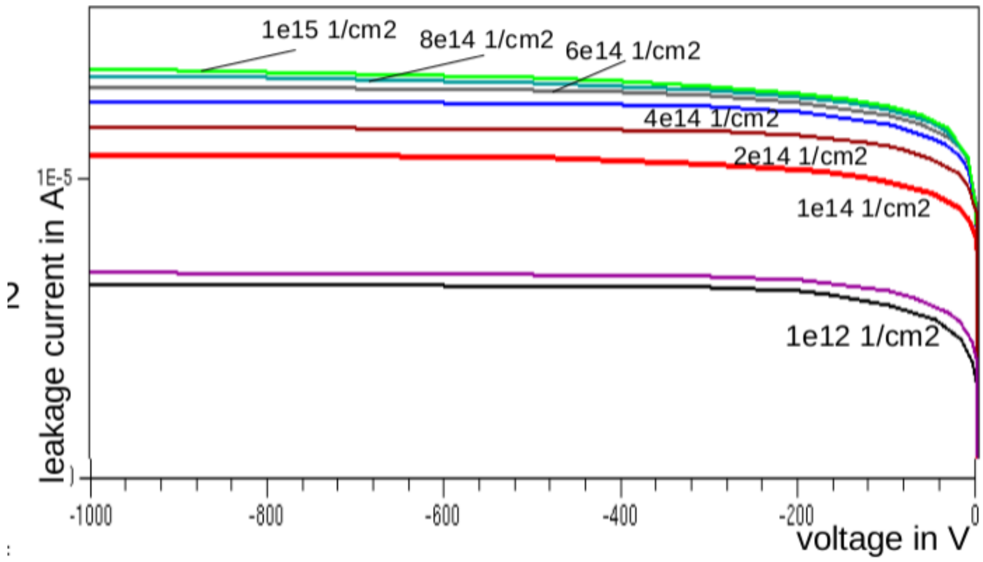

Figure 19: Leakage current vs voltage with Sentaurus Inspect

According to previous measurements, the increase of current is expected to be linear:

$$\frac{\Delta I}{V} = \alpha \Phi_{eq}$$

with:

$$\alpha \approx 10^{-17}$$

In order to test whether the sensor implemented with the trap model is working in the right way, it's necessary, first, to verify, for every simulation, whether the increase of current is linear and then to get the alfa value from the slope and check if it is in the expected order of magnitude. In the following diagram (Figure.20)current intensity has been taken at a voltage of 600V, nevertheless the same behavior can be seen for every simulated voltage level. The results of alfa values calculation are reported in the table of Figure.21.

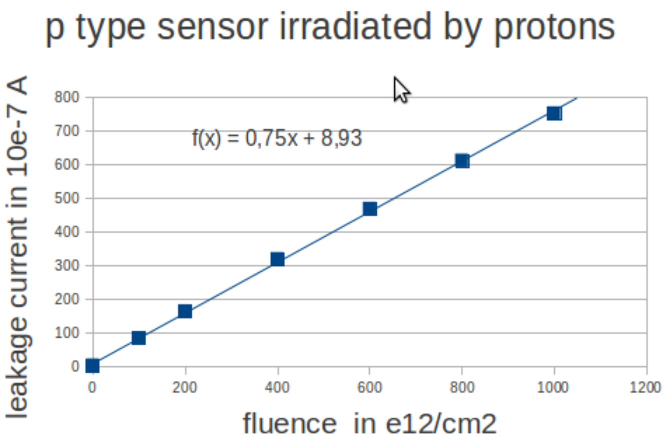

Figure 20: Leakage cuurent vs fluence at 600V

Sensor	Radiation	α in A/cm
p type	proton	$10\ e^{-17}$
	neutron	$9\ e^{-17}$
n type	proton	$12\ e^{-17}$
	neutron	$5\ e^{-17}$

Figure 21: alfa values

Since for every simulation the alfa constant is in the expected order of magnitude we can assume that the radiation damage effect is well reproduced by the implemented trap model.

4.2.2 Electric field

The next physical property to be analyzed is electric field. From previous measurements we expected it to change with fluence, following two different profiles.

At first, for lower fluence values, it is expected to keep a linear profile, the same as in unirradiated sensors, with an increase of the absolute value of the higher peak (Figure.22):

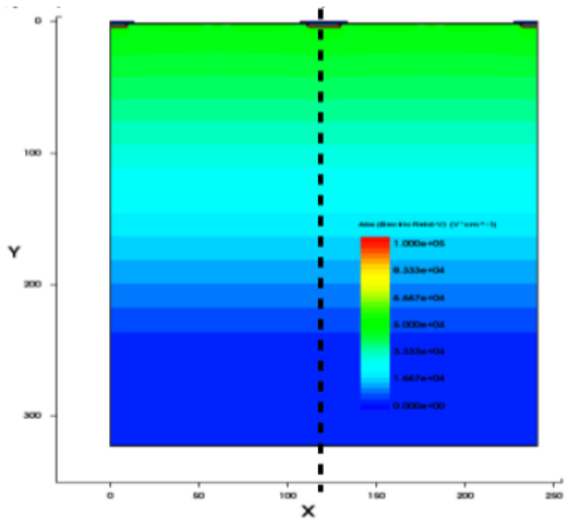

Figure 22: Electric field-Linear profile, with Sentaurus Visual

Then, with the increase of fluence, the previously mentioned double peak is expected to be seen (Figure.23):

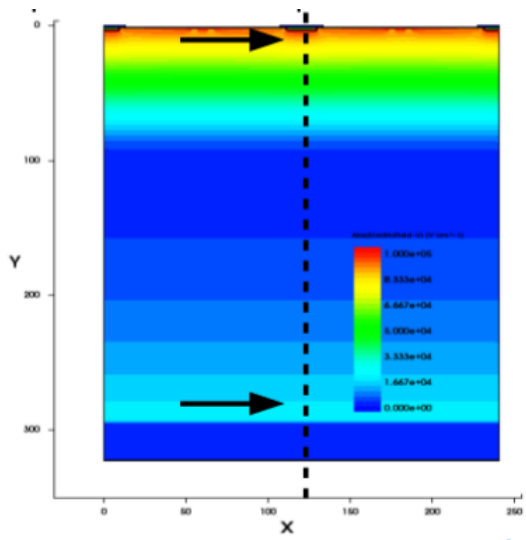

Figure 23: Electric double peak profile, with Sentaurus Visual

In order to study in which conditions the double peak can be observed, again different kind of sensors and irradiations have been simulated. The aim is to study how the electric field profile along the dashed line changes with fluence. In the following diagrams we can see the electric field vs sensor thickness (y position) for different fluence values.

As a first analysis, it might be useful to compare the two following diagrams(Figure.24, Figure.25). They refer to simulations of the sensors with the same thickness of active region irradiated by protons.

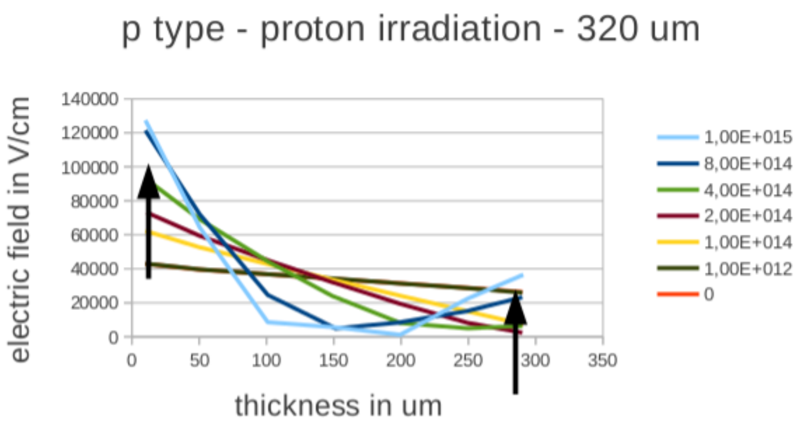

Figure 24: p type-proton radiation-320 μm

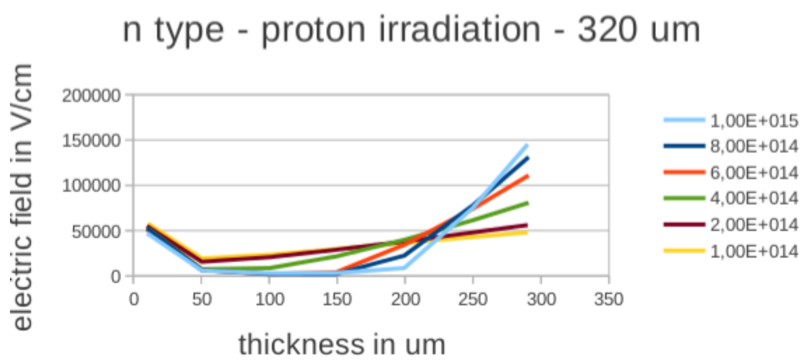

Figure 25: n type-proton radiation-320 μm

In this way sensors with different type of doping can be compared: the double peak can be always observed in n-type sensors (for every simulated fluence level), only for high fluence values in p type).

Further results can be taken analyzing two more plots (Figure.26, Figure.27):

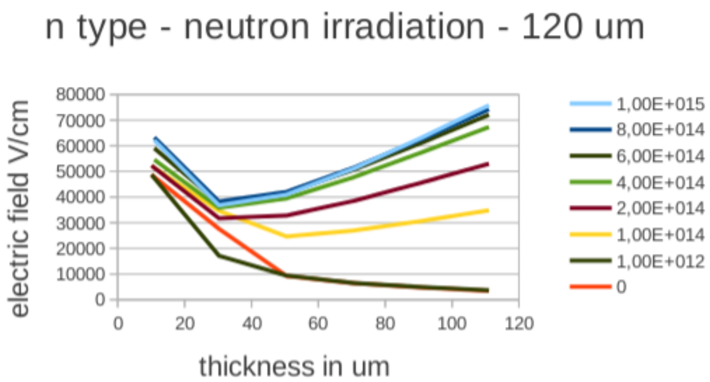

Figure 26: p type-neutron radiation-120 μm

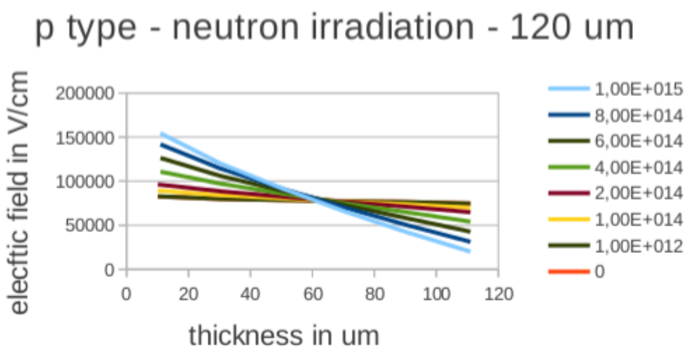

Figure 27: n type-neutron radiation-120 μm

1. through these simulations it is not possible to see significant differences between proton and neutron radiation effects;
2. in p-type sensor electric field is in general higher than in n-type;
3. the double peak can be observed, for fluence between 1e14 and 1e15, in n-type sensors with both 120 um and 320 um thickness of active region;
4. Concerning p-type sensors, the double peak is shown by thick sensors only for high fluence. It can be avoided in thinner sensors;

5 Summary and outlook

Through these simulations we have got the following results:

1. The general behave of the sensor doesn't depend on charges accumulate in the oxide layer. A change of physical properties is seen by increasing charge concentration in the $Si - SiO_2$ interface.

    (a) The increasing of the amount of charges doesn't effect the leakage current but only electric field.

    (b) Concerning capacitance the only one which shows a significantly variation is interstrip capacitance. Of these two properties we got the plots necessary to describe the dependence from charge concentration.

2. As far as radiation damage in silicon bulk is concerned sensors implemented with a trap model has been simulated.

    (a) From the behave of leakage current, which shows the expected increase, we now that the model we are using is working very well as a first approximation of the trap phenomenon.

    (b) The double peak effect of electric field has been reproduced, for n type sensors. Is not to be seen in thin p type sensors, only in thick sensors for high fluence values.

3. Future work will concern comparison with laboratory measurements.the general behave of the sensor doesn't depend

6 References

1. V Eremin, E. Verbitskaya and Z. Li, The origin of double peak elecric field distribution in heavily irradiated silicon detectors, Nucl. Instrum. Meth. A, 476(1):556-564, 2002

2. G Hohler, Karlsruhe, Springer Tracts in modern Physics Volume 231